



ELSEVIER

Available online at [www.sciencedirect.com](http://www.sciencedirect.com)**ScienceDirect**

Acta Materialia 88 (2015) 232–244



# Origin of the twinning to slip transition with grain size refinement, with decreasing strain rate and with increasing temperature in magnesium

C.M. Cepeda-Jiménez,\* J.M. Molina-Aldareguia and M.T. Pérez-Prado

IMDEA Materials Institute, C/Eric Kandel, 2, 28906 Getafe, Madrid, Spain

Received 19 December 2014; revised 16 January 2015; accepted 19 January 2015

Available online 13 February 2015

**Abstract**—The aim of this paper is to elucidate the origin of the transition from twinning to slip dominated flow in pure Mg. With that purpose, two polycrystals with average grain sizes of 19 and 5  $\mu\text{m}$  were prepared by rolling and annealing and they were tested in compression along the rolling direction at strain rates ranging from  $10^{-3}$  to  $10^{-5} \text{ s}^{-1}$  and at temperatures comprised between 50 and 250 °C. Twinning was evaluated by conventional electron backscatter diffraction (EBSD) and the activity of different slip systems was measured by an exhaustive EBSD-assisted slip trace analysis. A transition from twinning to basal slip, localized along deformation bands, was found to take place with decreasing grain size, with decreasing strain rate and with increasing temperature. The emergence of basal slip as the dominant deformation mechanism is promoted in all three cases by increasing levels of connectivity between favorably oriented grains, which facilitate slip transfer across grain boundaries. Such connectivity is related to the fraction of grain boundaries (GBs) with misorientations smaller than a threshold value ( $f_\theta < \theta_{\text{th}}$ ) as well as to their local arrangement. Since processing for grain refinement results in larger  $f_\theta < \theta_{\text{th}}$  values and both decreasing strain rate and increasing temperature increase  $\theta_{\text{th}}$ , in all cases twinning is eventually replaced by basal slip.

© 2015 Acta Materialia Inc. Published by Elsevier Ltd. All rights reserved.

**Keywords:** Twinning; Grain size; Temperature; Strain rate; Trace analysis

## 1. Introduction

Mechanical twinning has been recognized as a key deformation mechanism in metallic materials [1]. Its role is especially important in hexagonal closed packed (hcp) polycrystals in which, at low temperatures, dislocation slip alone might not provide the five independent systems required for intergranular strain compatibility [2].

Furthermore, in hcp metals in which the c/a ratio is larger than the ideal value of 1.633, such as magnesium and its alloys, the room temperature critical resolved shear stress (CRSS) of tensile twinning is commonly lower than that of non-basal slip systems [3–5] and, thus, strain accommodation by twinning might be preferred even when a sufficient number of slip systems are potentially available. Despite the intense efforts devoted over the years to understand this intriguing deformation mechanism, many fundamental issues remain, to date, unclear. For example, the influence on twinning of microstructural parameters such as the average grain size ( $d$ ), as well as of testing conditions like strain rate and temperature, are still not well understood. This paper focuses, in particular, on tensile twinning, which will be hereafter referred to as “twinning”.

The effect of grain size on twinning in magnesium at room temperature and quasi-static rates is still under debate [5–20]. First, although it is generally accepted that grain refinement gives rise to larger increases in the yield stress ( $\sigma_y$ ) when twinning is the main deformation mechanism than when dislocation slip prevails [6–8], several conflicting views have been put forth regarding the nature of such grain size dependence. On the one hand, the grain size effect on yielding during twin-dominated straining has been modeled using a Hall–Petch (HP) type relation ( $\sigma_y = \sigma_0 + kd^n$ ), where  $\sigma_0$ , the lattice friction stress, and  $k$ , the HP slope, vary widely with composition, texture, temperature and processing method [6–15]. This approach has, however, been recently called into question by a systematic statistical analysis of a large number of crystallites in a rolled high purity Mg polycrystal by Beyerlein et al. [16], who found no influence of grain size on whether or not at least one twin appeared in a specific grain. Second, the effect of  $d$  on the room temperature twinning activity is also still controversial. Some studies report a decrease of the twinning activity with grain refinement [7,17,18] as well as the occurrence of a twin to slip-dominated flow transition at a sufficiently low  $d$  value [7,19–21]. Different transition grain sizes have indeed been reported for Mg polycrystals processed using different methods. For example, Li et al. [19] observed the suppression of twinning for  $d$  values smaller than 2.7  $\mu\text{m}$  in pure Mg processed by equal channel angular

\* Corresponding author;

pressing (ECAP), Choi et al. [20] measured a transition grain size of 1  $\mu\text{m}$  in pure Mg samples fabricated by hot extrusion of ball-milled powders, and Chino et al. [21] found negligible twinning activity in an extruded AZ31 Mg rod when  $d = 8 \mu\text{m}$ . Other works, on the contrary, observe no variation in the twinning activity with grain refinement [22,23]. Ghaderi and Barnett [22] reported that the twin volume fraction during room temperature compression of an extruded AZ31 alloy along the extrusion axis (EA) remains invariant for grain sizes ranging from 5 to 55  $\mu\text{m}$ . Muránsky et al. [23] also measured the same twinned fraction in an extruded ZM20 alloy with  $d$  values comprised between 17 and 114  $\mu\text{m}$  under similar testing conditions. Finally, Wu et al. [24] reported the presence of twins in a ball-milled nanocrystalline Mg-10 at.% Ti with an average grain size as small as 33 nm. The effect of grain size on twinning is, clearly, still an open question that needs further clarification.

Testing conditions such as strain rate and temperature are also known to alter dramatically the twinning activity [1,5,7,25–35]. In particular, decreasing the strain rate and/or increasing the deformation temperature hinder twin activation to such an extent that, at a constant strain rate, twinning might be suppressed at sufficiently low temperatures and conversely, at a constant temperature, twin activation ceases below a critical strain rate [34]. The rationale behind these observations is that the CRSS for twinning is less sensitive to strain rate and temperature than that of slip [5] and this is reportedly consistent with the large core width ( $w$ ) predicted for  $\{10\bar{1}2\}$  zonal twinning dislocations ( $w = 6a$ ) [1]. Indeed, the CRSS of tensile twinning has been shown to remain basically constant at strain rates ranging from  $10^{-4}$  to  $10^3 \text{ s}^{-1}$  and at temperatures comprised between room temperature and 300 °C [3,6,7,27,34–36]. It is generally believed that, with increasing temperature, twinning is gradually replaced by non-basal slip, as it is known that the CRSSs of prismatic and pyramidal systems decrease rapidly with temperature [3,36]. However, the nature of the actual slip mechanism that replaces twinning at high temperatures or, for that matter, at low strain rates, has never been measured directly. The reason for this is that transmission electron microscopy (TEM) which is, to date, the most widely used experimental characterization technique to obtain *direct* evidence of the relative activity of different slip systems [37], does not yield sufficient statistics in coarse-grained polycrystals. This knowledge gap precludes a good understanding of the fundamental basis behind the observed dependence of twinning on strain rate and temperature.

The aim of this work is to clarify the origin of the twinning- to slip-dominated flow transition in pure Mg with decreasing grain size, decreasing strain rate and increasing temperature. With that purpose, several hot rolled pure Mg polycrystals with different grain sizes are compressed in-situ along the rolling direction (RD) at temperatures ranging from 50 to 250 °C and at strain rates comprised between  $10^{-5}$  and  $10^{-3} \text{ s}^{-1}$ . The slip and twin activities are estimated by electron-backscattered diffraction (EBSD)-assisted trace analysis. Denuded efforts were devoted to measure a large number of traces, in order to ensure the reliability of the study. Twin and slip activities are related to the corresponding microstructure and to the testing conditions, and are discussed in the frame of the existing literature.

## 2. Experimental procedure

The material employed in the current work was commercial high quality pure magnesium (99.95%), which was received as a 10 cm diameter ingot in the as-cast condition. Slabs of the as-received material with ~10 mm in thickness and ~30 mm in width were processed by hot rolling at 200 °C using three passes, each of 50% reduction, to a final thickness of ~3 mm. Post-processing heat treatments at 300 °C for 5 min and at 150 °C for 10 min were then carried out in order to generate two microstructures with  $d = 19 \mu\text{m}$  and  $d = 5 \mu\text{m}$ , respectively. The dominant basal textures as well as the GB misorientation distributions are very similar in both polycrystals, as demonstrated in a previous publication [38].

The microstructure and the crystallographic texture of the two rolled and annealed samples were examined by scanning electron microscopy (SEM) and EBSD using a field emission gun SEM (Helios NanoLab 600i, FEI) equipped with an HKL EBSD system, a CCD camera and the Channel 5.0 data acquisition and analysis software package. EBSD measurements were conducted at an accelerating voltage of 15 kV and 2.7 nA, using different step sizes depending on the sample grain size (0.2–1.5  $\mu\text{m}$ ). The average grain size values were calculated by the linear intercept method from EBSD maps in the normal direction to the rolling plane (ND) using only grain boundaries with misorientation angles greater than 15°. Sample preparation for EBSD included mechanical mirror-polish using first diamond pastes of increasingly finer particle sizes and then a colloidal silica slurry finishing. Finally, a chemical polish was performed for 5 s using a solution comprising 12 ml HCl, 8 ml HNO<sub>3</sub> and 100 ml methanol.

A series of dog-bone compressive samples with 10 mm gage length and transversal section of  $2 \times 2.5 \text{ mm}^2$  were electrodischarge-machined out of the two rolled and annealed sheets with the compression axis parallel to the rolling direction (RD). Compression tests were then carried out in the two polycrystals at 50 °C and  $10^{-3}$  using a screw-driven tensile stage (Kammler and Weiss, Dortmund, Germany) in order to analyze the effect of grain size on their macro and micromechanical response. The testing temperature was reached and maintained using a tungsten-based heater located just below the gage section of the sample. With the aim of investigating the effect of strain rate on the dominant deformation mechanisms additional compression tests were carried out in the same samples at 50 °C and at initial strain rates of  $10^{-4}$  and  $10^{-5} \text{ s}^{-1}$ . A second set of prism-shaped compression samples with 4 mm gage length along RD and  $2 \times 2 \text{ mm}^2$  section were also machined out of the rolled and annealed sheets in order to evaluate the influence of temperature. With that purpose, tests were performed at 50, 150, and 250 °C and at an initial strain rate of  $\sim 10^{-3} \text{ s}^{-1}$ . These compression tests were carried out in a Servosis universal testing machine equipped with a four-lamp ellipsoidal furnace. Under all the testing conditions mentioned above, some tests (two per sample) were performed to failure in order to characterize the full mechanical response and others were stopped at a strain of ~10%, at which the operating deformation mechanisms were carefully evaluated by the methodology described below.

The activation of different slip systems during compression testing at different temperatures and strain rates was

examined in the two polycrystals investigated by EBSD-assisted slip trace analysis [39,40]. This approach makes use of SEM images and EBSD orientation data input into a MATLAB code [41]. The basic steps of this methodology are the following. First, one surface of each compression sample must be perfectly polished in order to facilitate the post-test imaging of a vast number of slip traces. Large areas within the gage length are mapped by EBSD before and after each compression test, with the aim of analyzing the evolution of the orientations of the grains in which slip traces become apparent during straining. The assignment of each slip trace detected by SEM examination to a specific slip system is carried out by inputting the Euler angles of the corresponding grain (measured from the post-mortem EBSD maps) into a MATLAB code, which provides as output a visual representation of all the possible plane traces corresponding to that particular orientation [41]. Comparison of the slip trace under study with those simulated by the code allows selecting the actual active slip system. In general only one slip trace (or one set of parallel slip traces) was detected for each grain and no noticeable trace rotation was apparent until the macroscopic strain at which the slip trace analysis was carried out ( $\sim 10\%$ ). The activation of twinning during deformation at the different temperatures and strain rates investigated was tracked using conventional EBSD examination. The twin fraction has been estimated by calculating the fraction of grains that exhibit at least one twin within a given representative area. The Schmid factors (SF) for the slip and twin systems found to be active in each grain were calculated taking into account the corresponding pre-test EBSD-determined Euler angles and under the assumption of uniaxial stress along RD.

### 3. Results and discussion

#### 3.1. Twinning to slip transition with decreasing grain size

The true stress–true strain response during compression along RD at 50 °C and  $10^{-3} \text{ s}^{-1}$  of the two pure Mg polycrystals under study is represented in Fig. 1. The characteristic concave-up nature of the flow curve of the polycrystal with  $d = 19 \mu\text{m}$ , which is regarded as a manifestation of twinning-dominated plastic deformation following yielding, has been widely reported in the literature [13,16,22,31,42–44]. The plateau of constant stress apparent at low strains was attributed earlier to the formation of Lüders bands containing high amount of twinned grains, which progressively extend across the gage length of the compression sample [45]. The high degree of work hardening has been associated to crystal reorientation due to twinning and to strong dislocation-twin boundary interactions [7,46]. The stress–strain curve corresponding to the polycrystal with  $d = 5 \mu\text{m}$  (Fig. 1) exhibits, on the contrary, a concave-down shape typical of slip-dominated flow. As expected, the average yield strength ( $\sigma_{0.2}$ ) increases with decreasing grain size. In summary, in agreement with earlier works in the literature [7,19–21], the change in the shape of the true stress–true strain curves with decreasing grain size seems consistent with a twinning to slip dominated flow following yielding.

Estimating the dominant deformation mechanism solely from the shape of the macroscopic stress–strain curves is, however, a very rough approach. Thus, the microstructure and the microtexture of the two pure Mg polycrystals

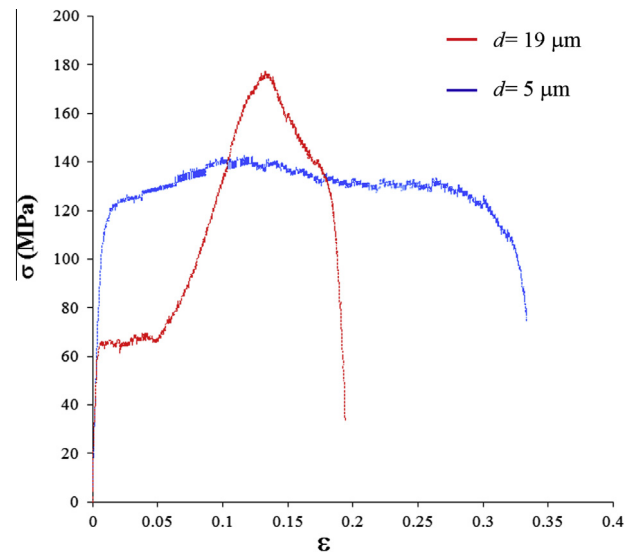


**Fig. 1.** Compressive true stress–true strain curves corresponding to pure Mg polycrystals with  $d$  values of 19 and 5  $\mu\text{m}$  deformed at 50 °C and at an initial strain rate of  $10^{-3} \text{ s}^{-1}$ .

investigated were characterized before and after straining in order to provide further insights on the operation of different deformation mechanisms at a microscopic scale. Fig. 2a and b illustrate the EBSD inverse pole figure (IPF) maps in the ND as well as the {0001} pole figures corresponding to the deformed gage of the polycrystal with  $d = 19 \mu\text{m}$  before testing as well after compression at 50 °C and  $10^{-3} \text{ s}^{-1}$ . An SEM micrograph of the same area is plotted next to the EBSD maps (Fig. 2c). In the as-processed condition, this polycrystal exhibits a strong basal texture, with a maximum intensity of  $\sim 12$  times random [38]. After straining, however, a new intensity maximum close to RD appears in the {0001} pole figure, in full agreement with previous experimental and modeling studies [5], due to lattice reorientation ( $\sim 86^\circ$ ) by tensile twinning. Indeed, it can be clearly seen in both the EBSD maps and the SEM micrograph of Fig. 2a–c that parallel bands containing a large fraction of twinned grains develop. The fraction of twinned grains is 60% (Fig. 2b). The formation of these so called Lüders bands was attributed to enhanced twin nucleation and propagation in neighboring grains with a high degree of connectivity in order to relax the local boundary stresses [23,45]. Fig. 2d, e and g are additional SEM micrographs at different magnifications after straining. In agreement with the mentioned previous study [45], Fig. 2e illustrates how twins (black arrows) inside the Lüders bands are connected at grain boundaries. Furthermore, this figure reveals the presence of slip traces dispersed within the bands (red arrows). An exhaustive EBSD-assisted analysis of 158 slip traces revealed that 79% corresponded to basal slip, 10% to prismatic  $\langle a \rangle$  slip, and 11% to pyramidal  $\langle c+a \rangle$  slip. Fig. 2g depicts incipient twin nucleation and propagation in the areas between two Lüders bands. No slip traces were detected in these regions. The SF distributions with respect to the global external stress corresponding to the twins detected both inside and outside the Lüders bands, together with the corresponding {0001} discrete pole figure showing the orientation of the  $c$ -axes of the twinned grains are plotted, respectively, in Fig. 2f and h. The SF histogram

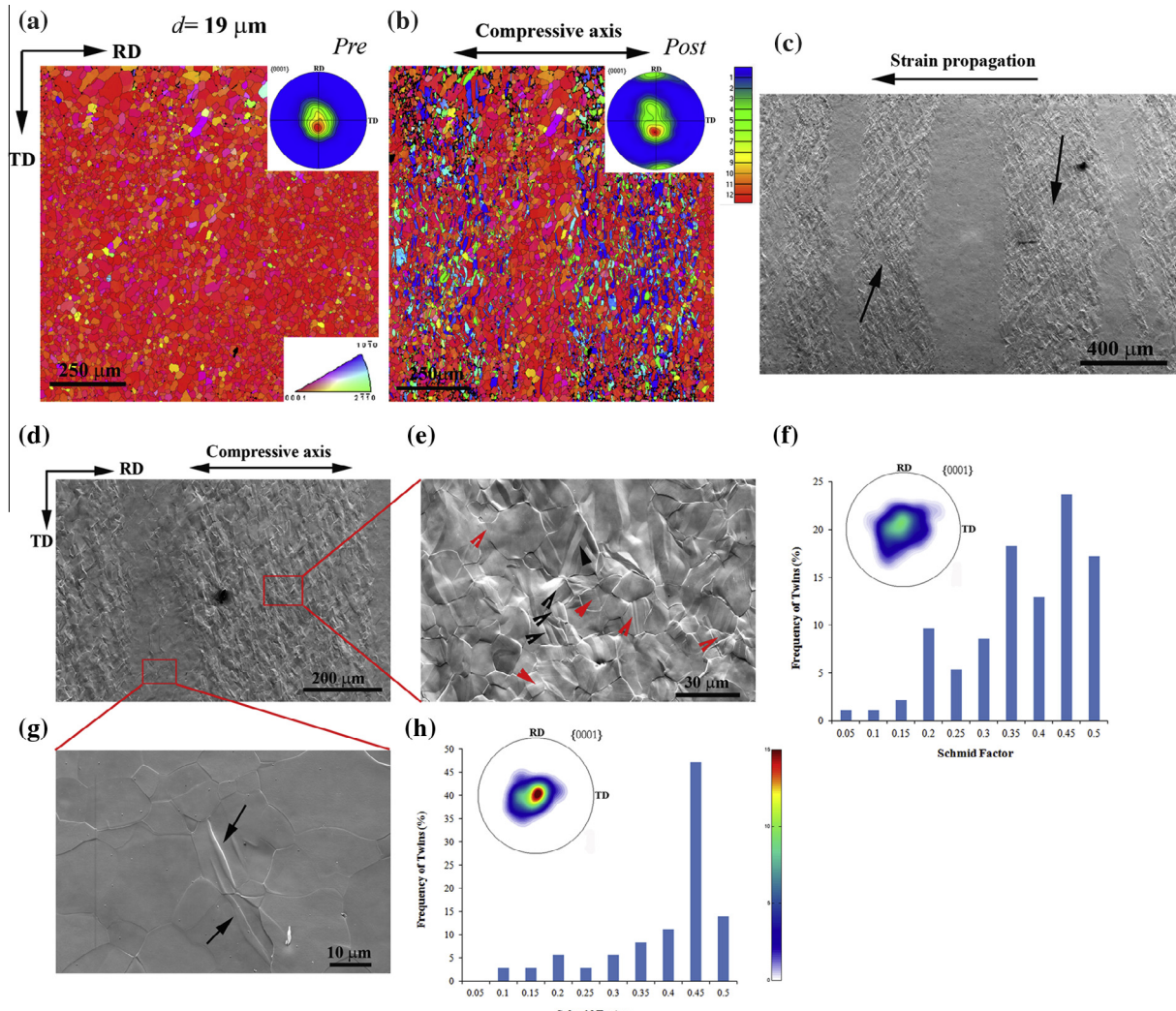


**Fig. 2.** (a and b) EBSD IPF maps in the ND and {0001} pole figures corresponding to the polycrystal with  $d = 19 \mu\text{m}$  (a) before testing and (b) after a strain of  $\sim 10\%$  at  $50^\circ\text{C}$  and  $10^{-3} \text{ s}^{-1}$ . (c and d) SEM micrographs showing the presence of highly twinned bands; (e and f) detailed characterization of twinning within the twin bands; (e) high magnification SEM micrograph and (f) SF<sub>twinning</sub> distribution and {0001} pole figure illustrating the  $c$ -axis corresponding to the twinned grains; (g and h) detailed characterization of incipient twinning outside the twin bands; (g) high magnification SEM micrograph and (h) SF<sub>twinning</sub> distribution of the twinned grains and the corresponding {0001} pole figure.

corresponding to areas within the bands (Fig. 2f) reveals that twinning took place in grains with both high and low SF, confirming that a significant fraction of twins was not activated in response to the applied stress but as a result of the need to accommodate GB stresses. Outside the Lüders bands (Fig. 2g) the few twins observed were mostly detected in grains with high SF in response to the applied stress (Fig. 2h). Altogether, the above observations confirm that, in the polycrystal with  $d = 19 \mu\text{m}$ , twinning is the dominant deformation mechanism following yielding at  $50^\circ\text{C}$  and  $10^{-3} \text{ s}^{-1}$ . Twinning takes place along bands as a response to the applied stress, first in grains with high SF. Subsequently, GB stresses emerging from twin-GB interactions are released by further twinning in grains with lower SF [1,5,47] and by slip.

Fig. 3a and b illustrates the EBSD IPF maps in the ND as well as the {0001} pole figures corresponding to the deformed gage of the polycrystal with  $d = 5 \mu\text{m}$  before testing as well as after compression along RD at  $50^\circ\text{C}$  and  $10^{-3} \text{ s}^{-1}$ . Again, in the as-processed condition, this

polycrystal exhibits a strong basal texture, with a maximum intensity of  $\sim 12$  times random (Fig. 3a) [38]. After straining a very weak maximum appears close to RD in the {0001} pole figure. Indeed, the fraction of twinned grains is now only 14% (Fig. 3b). The SEM micrograph of the same area (Fig. 3c) reveals that in the pure Mg polycrystal with  $d = 5 \mu\text{m}$  strain tends to concentrate along deformation slip bands making an angle with the compressive axis. These bands can be clearly seen in the corresponding post-straining EBSD map (Fig. 3b) as non-indexed points. Further details about slip bands are provided by the SEM micrographs at different magnifications of Fig. 3d–h. In areas relatively far from the deformation band propagation front (Fig. 3d–f), the first few slip traces start to appear and to transfer to neighboring grains. Within the deformation bands a large concentration slip traces are present (Fig. 3g and h). Again, an exhaustive EBSD-assisted analysis of 139 slip traces contained within the bands revealed that 73% corresponded to basal slip, 13% to prismatic  $\langle a \rangle$  slip, and 14% to pyramidal  $\langle c+a \rangle$  slip. Fig. 3i reveals that the SF for basal slip (SF<sub>basal</sub>)

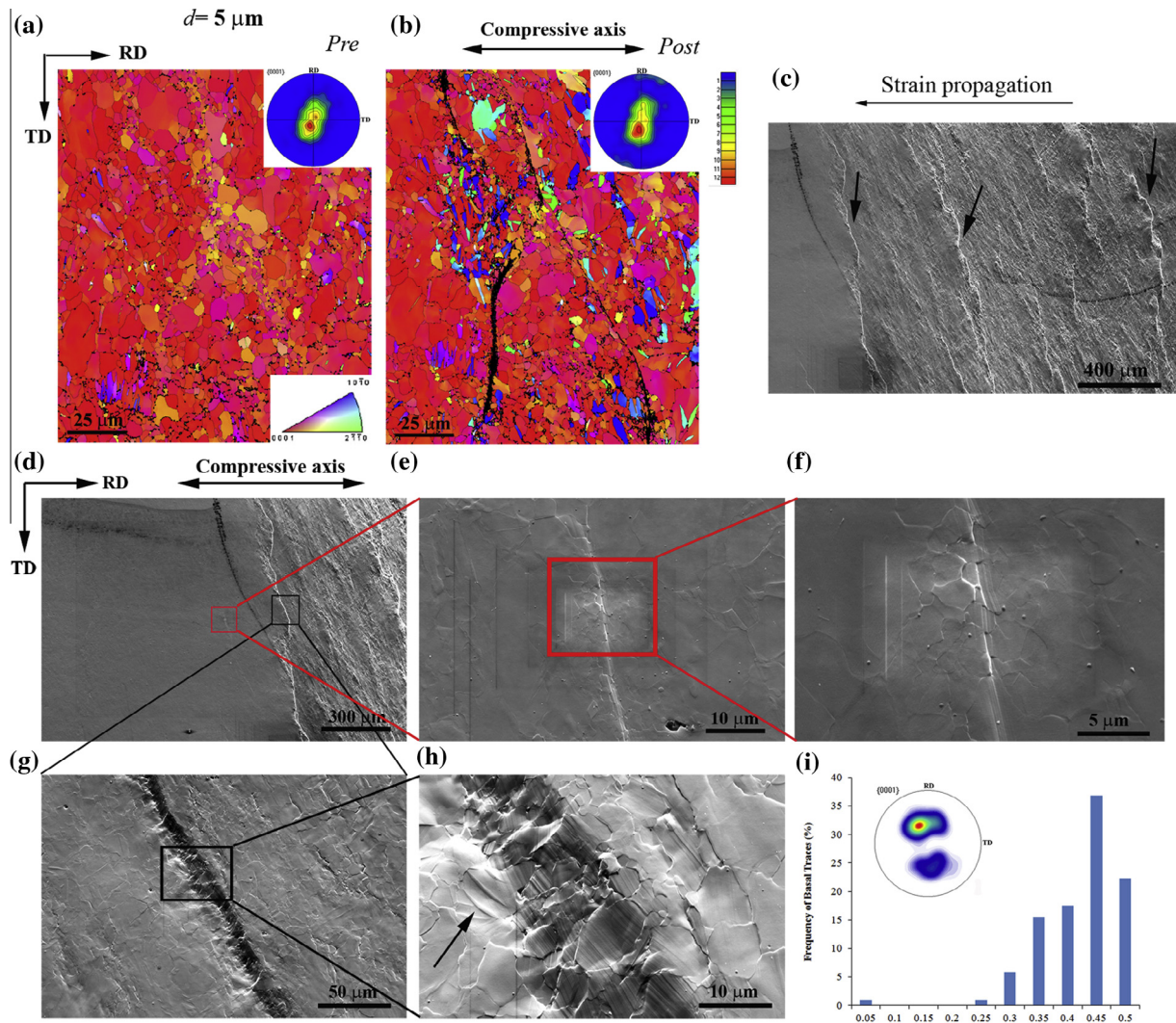


**Fig. 3.** (a and b) EBSD IPF maps in the ND and {0001} pole figures for the polycrystal with  $d = 5 \mu\text{m}$  (a) before testing and (b) after a strain of  $\sim 10\%$  at  $50^\circ\text{C}$  and  $10^{-3} \text{ s}^{-1}$ ; (c–h) SEM micrographs at different magnifications showing the microstructure within the bands; (i) SF<sub>basal</sub> distribution of the grains within the bands in which basal slip was observed and the corresponding {0001} pole figure.

corresponding to the grains contained within the bands are very high, indicating that this mechanism becomes active in response to the applied stress. Summarizing, basal slip, localized along well-defined bands, is the dominant deformation mechanism in the polycrystal with an average grain size of  $5 \mu\text{m}$  at  $50^\circ\text{C}$  and  $10^{-3} \text{ s}^{-1}$ . Altogether, and in agreement with the macroscopic mechanical stress–strain curves of Fig. 1, our microstructural study supports the occurrence of a twinning to basal slip dominated flow transition with decreasing grain size upon yielding.

The high activity of basal slip observed would not be expected due to the low average SF<sub>basal</sub> that is characteristic of rolled Mg alloys. In a previous publication on the tensile behavior at  $50^\circ\text{C}$  of these same polycrystals [38], the average SF<sub>basal</sub> were calculated using X-ray diffraction (XRD) and electron backscattered diffraction (EBSD). The corresponding XRD values were 0.230 ( $d = 19 \mu\text{m}$ ), and 0.240 ( $d = 5 \mu\text{m}$ ), and the EBSD values were 0.180 ( $d = 19 \mu\text{m}$ ), and 0.188 ( $d = 5 \mu\text{m}$ ). Therefore, both techniques confirm the resemblance of the macro and micro-texture as well as the presence of relatively poorly oriented grains for basal slip in the two pure Mg polycrystals investigated.

Accordingly, the formation of basal slip deformation bands in the fine-grained polycrystal can be rationalized as follows. Fig. 4 illustrates the misorientation angles ( $\theta$ ) of the GBs across which basal slip transfer could take place (blue bars) and of those at which slip traces were arrested (red bars). It can be clearly seen that  $\theta_{\text{th}} \sim 30^\circ$  is the upper limit for basal slip transfer. It appears, therefore, that even though the fraction of grains that are favorably oriented for basal slip in the rolled pure Mg polycrystals under study is small, when those grains are connected by boundaries with misorientation angles smaller than  $30^\circ$ , slip transfer takes place easily and, thus, basal slip prevails.

It is, therefore, at this point reasonable to hypothesize that the transition from twinning to basal slip-dominated flow with decreasing grain size could be caused by a change in the “connectivity” between grains that are favorably oriented for basal slip emerging from the processing. Indeed, some properties of polycrystals are known to depend on the topology of the GB networks and this dependence has been modeled using percolation theory concepts [48]. In order to test the validity of the above hypothesis a thorough study of the connectivity between grains that are

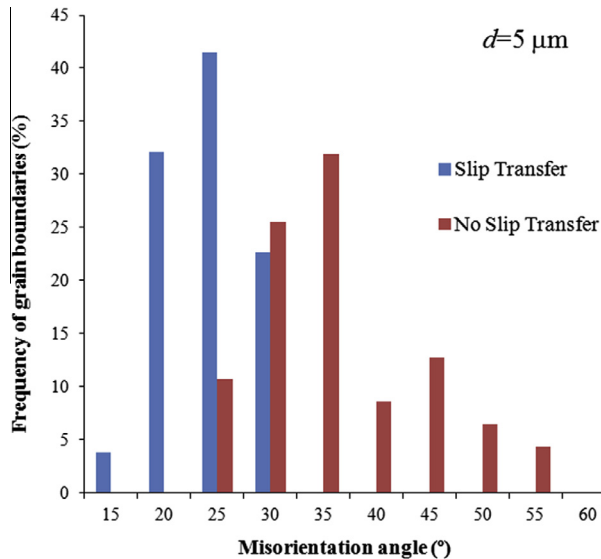


**Fig. 4.** Polycrystal with  $d = 5 \mu\text{m}$  tested at  $50^\circ\text{C}$  and  $10^{-3} \text{s}^{-1}$ . Misorientation distribution histogram of GBs inside the deformation bands across which basal slip transfer could take place (blue bars) and of those at which slip traces were arrested (red bars). (For interpretation of the references to color in this figure legend, the reader is referred to the web version of this article.)

favorably oriented for basal slip was performed in the two polycrystals investigated. The following assumptions have been made in order to carry out this analysis. Taking into

account that the initial CRSS for twinning is approximately twice that of basal slip [3] and since the average SF for twinning ( $\text{SF}_{\text{twinning}}$ ) in the two investigated polycrystals is  $\sim 0.4$ , a “grain well oriented for basal slip” has been defined as that in which  $\text{SF}_{\text{basal}} > 0.2$ . This seems a reasonable assumption since, as can be seen in Fig. 3i, the  $\text{SF}_{\text{basal}}$  of most grains within the deformation bands is larger than 0.2. Fig. 5 illustrates two large EBSD IPF maps in which grains with  $\text{SF}_{\text{basal}} > 0.2$  are highlighted in the pure Mg polycrystals with  $d = 19 \mu\text{m}$  (Fig. 5a) and  $d = 5 \mu\text{m}$  (Fig. 5b). The corresponding misorientation distribution histograms are depicted next to the EBSD maps. The basic state variable used in GB percolation problems is the fraction of special boundaries in the network [49]. Here, GBs with  $\theta < 30^\circ$  will be defined as “special” as they allow basal slip transfer. Thus, the degree of connectivity between the grains highlighted in Fig. 5 may be estimated, as a first approximation, by calculating the fraction of boundaries with  $\theta < 30^\circ$  ( $f_{\theta < 30^\circ}$ ) from the corresponding misorientation distribution histograms. The  $f_{\theta < 30^\circ}$  values for the two polycrystals with  $d = 19 \mu\text{m}$  and  $d = 5 \mu\text{m}$  are 63% and 73%, respectively. Although these data suggest that, indeed, the grains that are favorably oriented for basal slip are better connected in the finest polycrystal, the difference between both  $f_{\theta < 30^\circ}$  values is small. An additional measure of network connectivity, which takes into account that GBs of different types are not randomly distributed in the network, is the triple junction distribution, which gives information on the coordination of special GBs at triple junctions [49,50]. Fig. 6 shows GB misorientations maps corresponding to grains

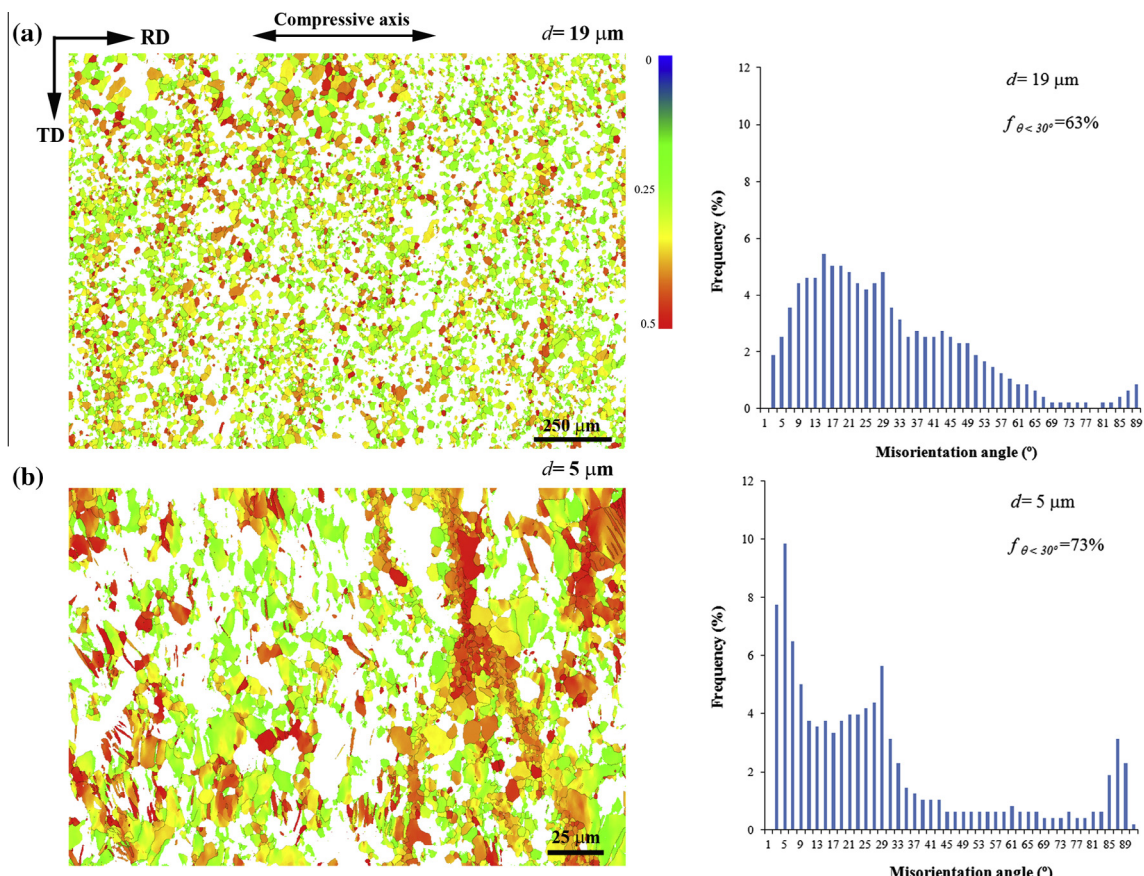


**Fig. 5.** EBSD maps showing the grains with  $\text{SF}_{\text{basal}} > 0.2$  in the polycrystals with (a)  $d = 19 \mu\text{m}$  and (b)  $d = 5 \mu\text{m}$  and, next to them, the corresponding misorientation distribution histograms.

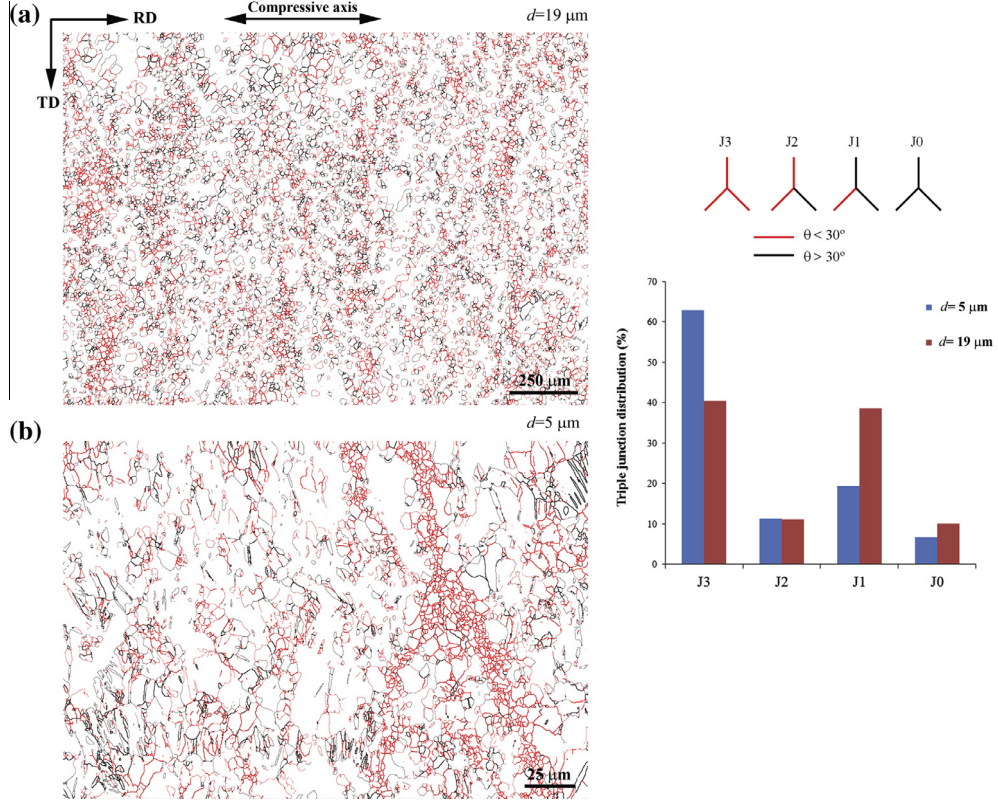


**Fig. 6.** GB maps corresponding to the EBSD SF maps of Fig. 5. (a)  $d = 19 \mu\text{m}$  and (b)  $d = 5 \mu\text{m}$ . GBs with  $\theta < 30^\circ$  are colored in red while GBs with  $\theta > 30^\circ$  are colored in black. The corresponding triple junction distribution histograms are also included. (For interpretation of the references to color in this figure legend, the reader is referred to the web version of this article.)

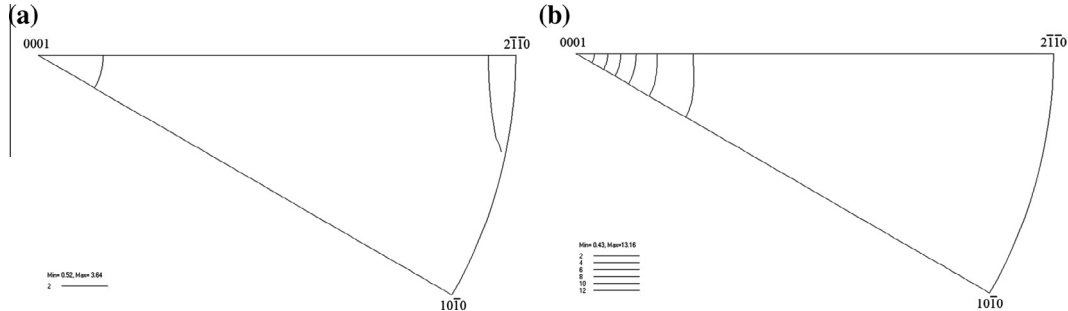


**Fig. 7.** Polycrystal with  $d = 5 \mu\text{m}$ . Misorientation axis distributions for boundaries with misorientation angles between  $2^\circ$  and  $30^\circ$  ( $\theta_{\text{th}}$ ) corresponding to (a) boundaries included in the area depicted in the EBSD map of Fig. 3a, and (b) boundaries inside the deformation bands across which basal slip transfer took place.

with  $SF_{\text{basal}} > 0.2$  for the two polycrystals (Fig. 6a for  $d = 19 \mu\text{m}$  and Fig. 6b for  $d = 5 \mu\text{m}$ ). Red and black lines represent boundaries with  $\theta < 30^\circ$  (special GBs) and with  $\theta > 30^\circ$  (general GBs), respectively. The corresponding triple junction distributions are also shown in Fig. 6.  $J_i$  junctions are those coordinated by  $i$  special boundaries [49]. The fraction of  $J_2$  and  $J_3$  junctions ( $f_{J_2+J_3}$ ) is 51% in the polycrystal with  $d = 19 \mu\text{m}$  and 74% in the polycrystal with  $d = 5 \mu\text{m}$ . This analysis reveals, first, that the degree of connectivity of grains that are well oriented for basal slip is higher in the finest polycrystal. Second, the present results support the existence of a threshold value of the fraction of special GBs beyond which strain is accommodated by basal slip along deformation bands. This behavior

resembles that reported earlier for *high contrast* properties, which depend strongly on the nature of the GB network [49].

Fig. 7 shows, furthermore, the distribution of misorientation axes for the special boundaries of the polycrystal with  $d = 5 \mu\text{m}$ . Fig. 7a corresponds to the boundaries included in the area depicted in Figs. 3a and 7b corresponds to the boundaries inside the deformation bands across which basal slip transfer took place. It can be seen that the misorientation angles of the boundaries that favor basal slip transfer are mostly parallel to the  $c$ -axis.

Thus, this work evidences that the origin of the transition between twinning and slip-dominated flow with decreasing grain size in pure Mg might be the larger

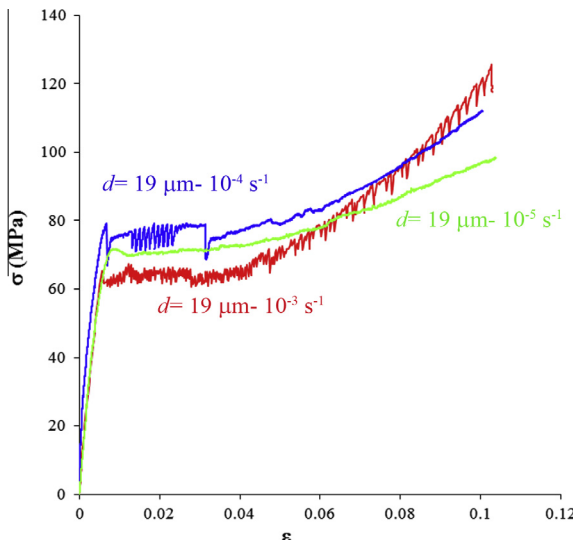


**Fig. 8.** Compressive true stress–true strain curves corresponding to the pure Mg polycrystal with  $d = 19 \mu\text{m}$  deformed at  $50^\circ\text{C}$  and at initial strain rates of  $10^{-3}$ ,  $10^{-4}$  and  $10^{-5} \text{ s}^{-1}$ .

fraction of “well-connected” clusters of grains favorably oriented for basal slip in the fine grained microstructures. It must be emphasized here that in a large majority of the studies aimed to analyze the influence of grain size on the mechanical behavior of Mg alloys [5–18,20–23,43,51–54] the samples with different  $d$  values are first processed by rolling or extrusion at moderate to elevated temperatures to avoid cracking, and then annealed to reach the desired average grain size value. Unavoidably, these processing routes lead to well known deformation textures, which have been exhaustively characterized [5]. To our knowledge, however, no studies in the past have quantified the correlations between the rolling and extrusion processing parameters and the percolation properties of the resulting GB networks in pure Mg and in Mg alloys. Nevertheless, it is known that clusters of grains well oriented for basal slip do form during rolling and extrusion of Mg alloys at low to moderate temperatures [55–57], while subsequent annealing at higher temperatures leads to the preferential growth of grains with  $c$ -axes parallel to the rolling plane or, respectively, perpendicular to the extrusion direction. Thus, it seems logical to presume that the connectivity of

the clusters of grains favorably oriented for basal slip decreases with increasing  $d$  in most of the works in which polycrystals were processed using these conventional processing routes, as demonstrated in the present study.

### 3.2. Twinning to slip transition with decreasing strain rate

**Fig. 8** shows the compression true stress–strain curves corresponding to the pure Mg polycrystal with  $d = 19 \mu\text{m}$  tested at  $50^\circ\text{C}$  and at initial strain rates of  $10^{-3}$ ,  $10^{-4}$  and  $10^{-5} \text{ s}^{-1}$ . In general, the three curves exhibit a plateau after yielding, followed by different levels of work hardening, the latter decreasing as the strain rate is reduced. In addition, the curves corresponding to strain rates of  $10^{-3}$  and  $10^{-4} \text{ s}^{-1}$  exhibit serrations, which are typically attributed to nucleation and propagation of twinning Lüders bands (**Fig. 2**) [1]. However, such serrated flow is absent from the curve corresponding to the lowest strain rate, suggesting a transition from twinning to slip dominated flow.

**Fig. 9** illustrates several representative SEM micrographs corresponding to the same polycrystal after compression at  $50^\circ\text{C}$  and at  $10^{-4} \text{ s}^{-1}$  (**Fig. 9a**) and  $10^{-5} \text{ s}^{-1}$  (**Fig. 9b**). Comparison of **Fig. 9** with **Fig. 2** allows analyzing the microstructural influence of strain rate on the microstructural evolution during straining. While at the highest strain rate twinning was clearly the dominant deformation mechanism (**Fig. 2**), when the strain rate is reduced down to  $10^{-4} \text{ s}^{-1}$ , both twinning and slip are apparent (**Fig. 9a**). At  $10^{-5} \text{ s}^{-1}$  (**Fig. 9b**) intense slip localization takes place along deformation bands. Out of the 119 slip traces analyzed in the polycrystal after compression at  $10^{-5} \text{ s}^{-1}$ , 91% corresponded to basal slip, 6% to prismatic  $\langle a \rangle$  slip, and 3% to pyramidal  $\langle c+a \rangle$  slip. At this strain rate the fraction of twinned grains is very low (8%), as observed in the corresponding EBSD IPF map after deformation (**Fig. 10**). Thus, these results evidence again a clear transition from twinning to basal slip dominated flow as the strain rate decreases from  $10^{-3}$  to  $10^{-5} \text{ s}^{-1}$  in the pure Mg polycrystal with  $d = 19 \mu\text{m}$ .

**Fig. 11a** illustrates the misorientation distribution histogram corresponding to GBs located within the deformation bands developed at  $10^{-5} \text{ s}^{-1}$  in the pure Mg polycrystal with  $d = 19 \mu\text{m}$ . GBs allowing slip transfer (blue) and arresting slip (red) are differentiated. It can be seen that  $\theta_{\text{th}}$  increased from  $30^\circ$  at  $10^{-3} \text{ s}^{-1}$  (**Fig. 4**) to  $45^\circ$  at  $10^{-5} \text{ s}^{-1}$ . This is consistent with a relaxation of constraints

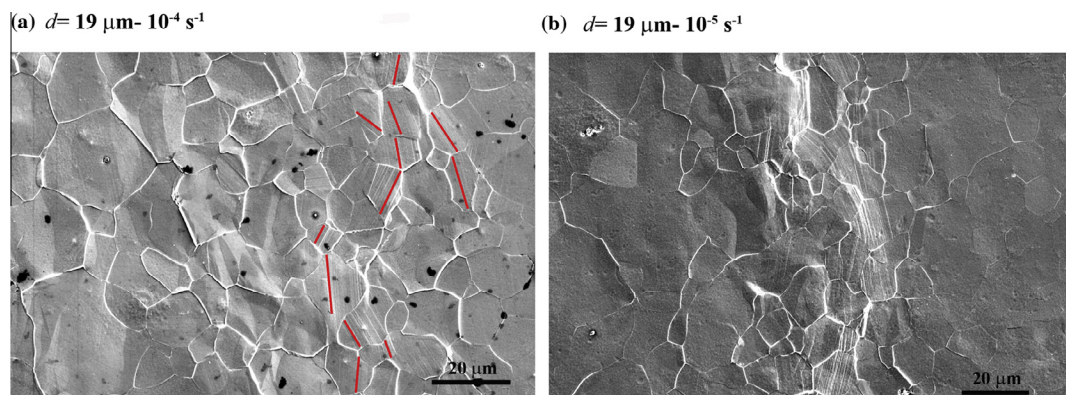


**Fig. 9.** SEM micrographs illustrating the microstructure of the polycrystal with  $d = 19 \mu\text{m}$  after compression at  $50^\circ\text{C}$  at: (a)  $10^{-4} \text{ s}^{-1}$  and (b)  $10^{-5} \text{ s}^{-1}$ .

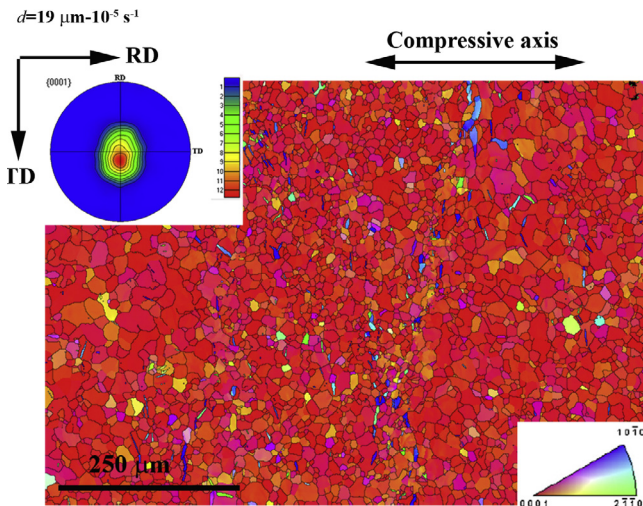


**Fig. 10.** EBSD IPF map in the ND and  $\{0001\}$  pole figure corresponding to the polycrystal with  $d = 19 \mu\text{m}$  after a compressive strain of  $\sim 10\%$  at  $50^\circ\text{C}$  and  $10^{-5} \text{ s}^{-1}$ .

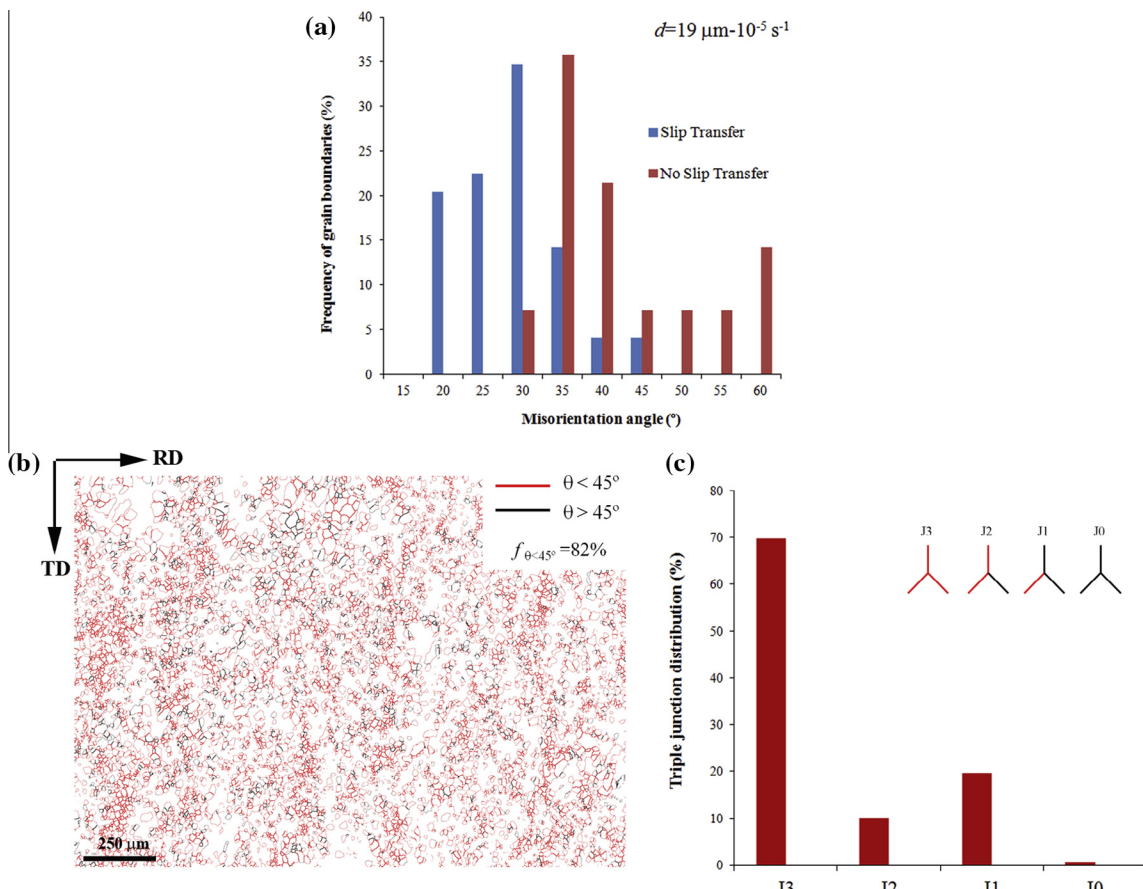
at GBs with decreasing strain rate. The connectivity between grains favorably oriented for basal slip, i.e. with  $SF_{\text{basal}} > 0.2$  (Fig. 11b) can be estimated by calculating

the fraction of boundaries with  $\theta < 45^\circ$  ( $f_{\theta < 45^\circ}$ ), which is 82%, and the fraction of  $J_2$  and  $J_3$  junctions ( $f_{J_2+J_3}$ ), which is 80% (Fig. 11c).  $f_{J_2+J_3}$  at  $10^{-5} \text{ s}^{-1}$  is significantly larger than at  $10^{-3} \text{ s}^{-1}$  (51%). Therefore, it is our contention that the transition from twinning to basal slip dominated flow that takes place at  $50^\circ\text{C}$  with decreasing strain rate in the pure Mg polycrystal with  $d = 19 \mu\text{m}$  may be attributed to the enhanced percolation of basal slip transfer between grains favorably oriented for basal slip.

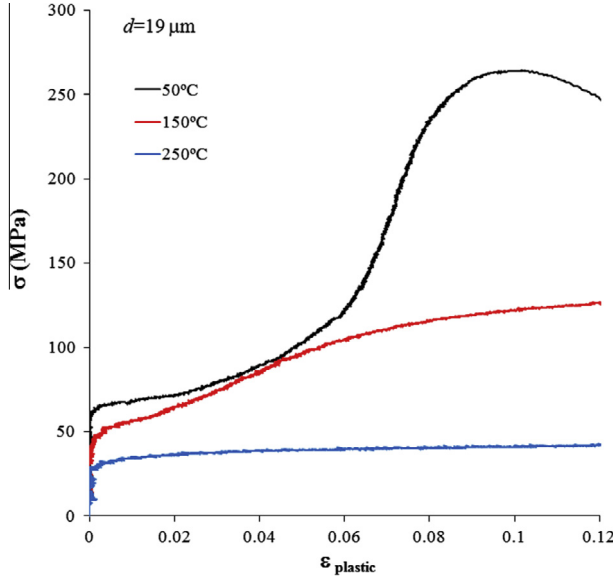
### 3.3. Twinning to slip transition with increasing temperature

Fig. 12 illustrates the compressive true stress-strain curves corresponding to the pure Mg polycrystal with  $d = 19 \mu\text{m}$  deformed at  $10^{-3} \text{ s}^{-1}$  and at  $50, 150$ , and  $250^\circ\text{C}$ . As expected, the yield stress ( $\sigma_{0.2}$ ) and the work hardening rate decrease progressively with increasing test temperature. In addition, the shape of the curve changes gradually from being concave-up at  $50^\circ\text{C}$  to concave-down at  $250^\circ\text{C}$ , consistent with a transition in the dominant deformation mechanism from twinning to slip as the temperature is raised.

Fig. 13a and b illustrates the EBSD IPF maps and the corresponding  $\{0001\}$  pole figures for the polycrystal with  $d = 19 \mu\text{m}$  after compression at  $150$  and  $250^\circ\text{C}$ , respectively. As expected, the fraction of twinned grains decreases



**Fig. 11.** Polycrystal with  $d = 19 \mu\text{m}$  tested at  $50^\circ\text{C}$  and  $10^{-5} \text{ s}^{-1}$ . (a) Misorientation distribution histogram of grain boundaries inside the deformation bands across which basal slip transfer could take place (blue bars) and of those at which slip traces were arrested (red bars); (b) GB map corresponding to the EBSD SF map of Fig. 5a. GBs with  $\theta < 45^\circ$  are colored in red while GBs with  $\theta > 45^\circ$  are colored in black. (c) The corresponding triple junction distribution histogram is also included. (For interpretation of the references to color in this figure legend, the reader is referred to the web version of this article.)



**Fig. 12.** Compressive true stress–true strain curves corresponding to the pure Mg polycrystal with  $d = 19 \mu\text{m}$  deformed at 50, 150 and 250 °C and at an initial strain rate of  $10^{-3} \text{ s}^{-1}$ .

notably with temperature, being 14% at 150 °C and almost negligible at 250 °C. Indeed, with increasing temperature, again, strain localization along deformation slip bands takes place. Fig. 13c and d consists of two SEM micrographs illustrating the deformation bands developed in

the pure Mg polycrystal with  $d = 19 \mu\text{m}$  after compression at  $10^{-3} \text{ s}^{-1}$  at 150 °C (Fig. 13c) and at 250 °C (Fig. 13d). EBSD-assisted slip trace analysis of, respectively, 154 and 76 traces, revealed that, at 150 °C, 78% corresponded to basal slip, 8% to prismatic  $\langle a \rangle$  slip, and 14% to pyramidal  $\langle c+a \rangle$  slip, while at 250 °C 61% corresponded to basal slip, 13% to prismatic  $\langle a \rangle$  slip, and 26% to pyramidal  $\langle c+a \rangle$  slip. Thus, these results confirm the occurrence of a transition from twinning to basal slip dominated flow when the temperature increases from 50 °C to 150° and to 250 °C. The increased contribution of non-basal slip at the highest temperature (250 °C) is consistent with the well-known decrease of the CRSS of prismatic and pyramidal  $\langle c+a \rangle$  systems with increasing temperature [31,36], as well as with the onset of substantial cross-slip from basal to non-basal planes (Fig. 14) [58].

Let's examine the transition from twinning to basal slip dominated flow at 150 °C. Fig. 15a illustrates the misorientation distribution histogram corresponding to GBs located within the deformation bands developed at 150 °C in the pure Mg polycrystal with  $d = 19 \mu\text{m}$ . GBs allowing slip transfer (blue) and arresting slip (red) are differentiated. It can be seen that  $\theta_{\text{th}}$  increased from 30° at 50 °C (Fig. 4) to 37° at 150 °C. This is, again, consistent with a relaxation of constraints at GBs with increasing temperature. The connectivity between grains favorably-oriented for basal slip, i.e. with  $SF_{\text{basal}} > 0.2$  (Fig. 15b) can be estimated by calculating the fraction of boundaries with  $\theta < 37^\circ$  ( $f_{\theta < 37^\circ}$ ), which is 72%, and the fraction of  $J_2$  and  $J_3$  junctions ( $f_{J_2+J_3}$ ), which is 63% (Fig. 15c). It can be seen that  $f_{J_2+J_3}$  at 150 °C is larger than at 50 °C (51%). Furthermore,

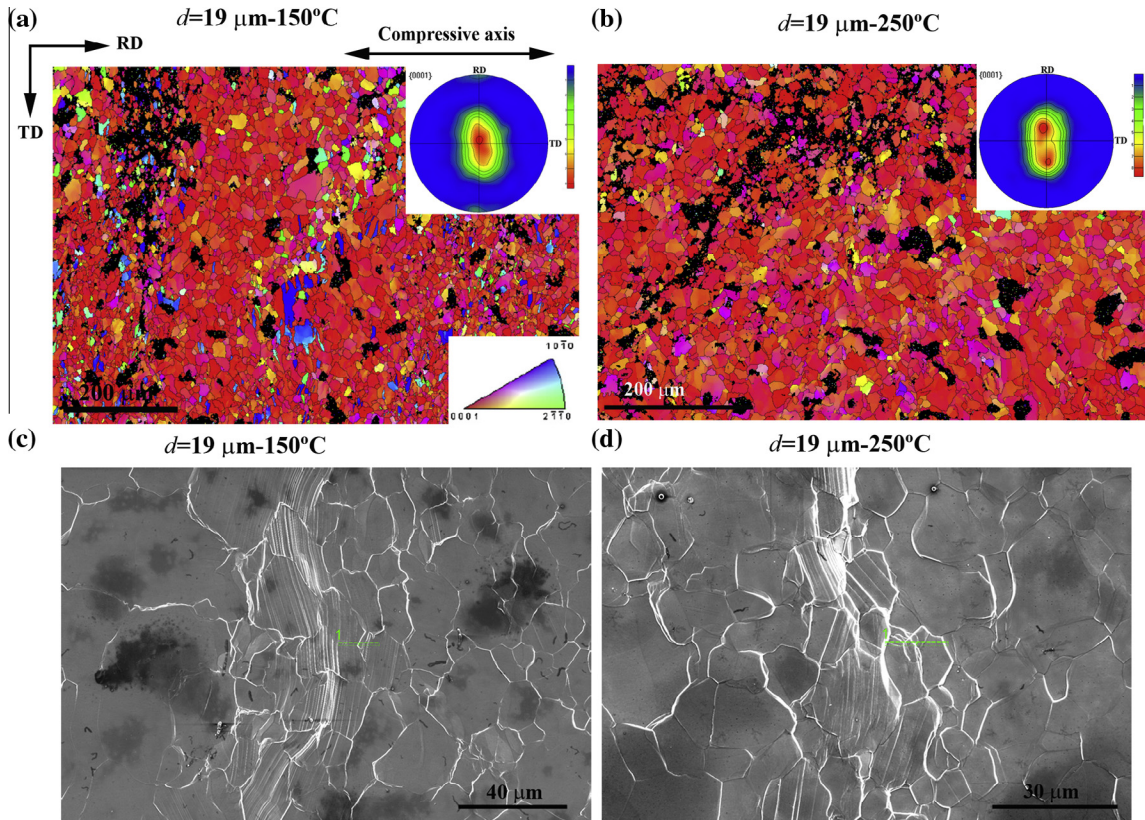


**Fig. 13.** (a and b) EBSD IPF maps in the ND and  $\{0001\}$  pole figures corresponding to the polycrystal with  $d = 19 \mu\text{m}$  after a strain of  $\sim 10\%$  at (a) 150 °C and (b) 250 °C; (c and d) SEM micrographs illustrating transfer of basal slip across GBs after compression at (c) 150 °C and (d) 250 °C.

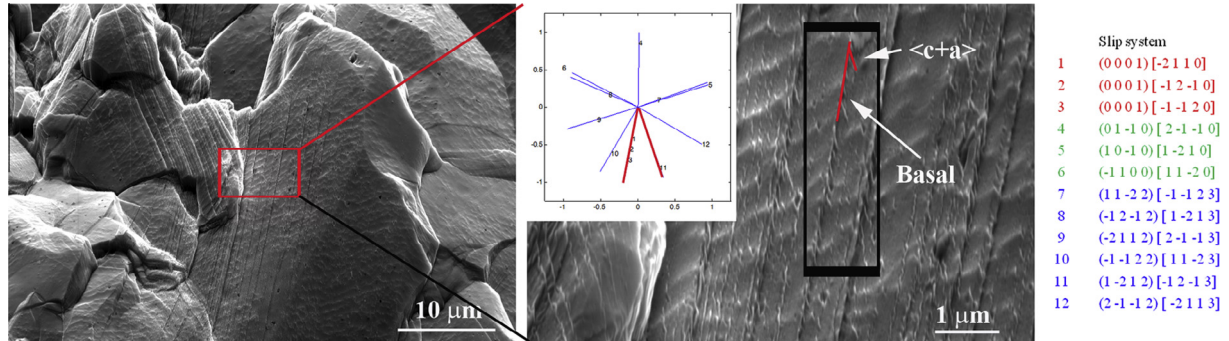


**Fig. 14.** SEM micrographs at two magnifications illustrating cross-slip of (a) dislocations from basal onto pyramidal planes during compression at 250 °C in the polycrystal with  $d = 19 \mu\text{m}$ .

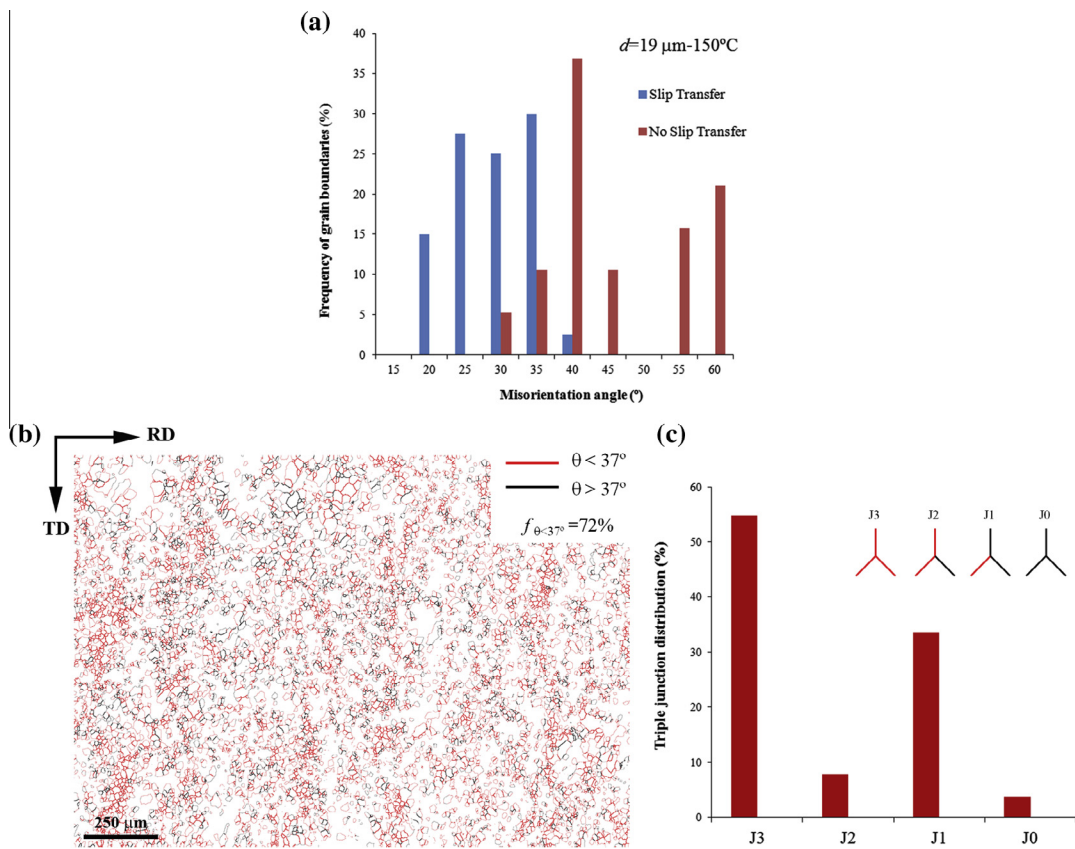


**Fig. 15.** Polycrystal with  $d = 19 \mu\text{m}$  tested at 150 °C and  $10^{-3} \text{ s}^{-1}$ . (a) Misorientation distribution histogram of grain boundaries inside the deformation bands across which basal slip transfer could take place (blue bars) and of those at which slip traces were arrested (red bars); (b) GB map corresponding to the EBSD SF map of Fig. 5a. GBs with  $\theta < 37^\circ$  are colored in red while GBs with  $\theta > 37^\circ$  are colored in black. (c) The corresponding triple junction distribution histogram is also included. (For interpretation of the references to color in this figure legend, the reader is referred to the web version of this article.)

these data suggest that the threshold  $f_{J2+J3}$  value required for the twinning to slip transition to take place might be comprised between 51% and 63%. Therefore, it is our contention that the transition from twinning to basal slip dominated flow that takes place with increasing temperature in the pure Mg polycrystal with  $d = 19 \mu\text{m}$  may also be attributed to the enhanced percolation of basal slip transfer between grains favorably oriented for basal slip.

### 3.4. Outlook

The current study evidences that the topology of the GB network, together with the local crystallographic orientations, play a decisive role in the selection of the dominant deformation mechanisms in pure Mg polycrystals. In particular, boundary percolation effects relative to basal slip transfer, which emerge from the processing and which

change with temperature and strain rate, are shown to be critical to determine the twinning to slip transition. It is foreseen that the same concept can be applied to Mg alloys and, for that matter, to hcp metals. The apparently contradicting reported evidences of the dependence of the occurrence of twinning with grain size [7,17–24] might be reconciled when the corresponding GB network topologies and spatial distribution of orientations are taken into account. Finally, our study suggests that models relating the average grain size with bulk mechanical properties, such as the HP law, should be taken with caution, as they ignore both the intrinsic nature of individual GBs, as well as their spatial distribution. The large scatter in the HP parameters found for Mg and its alloys [6–15] could, perhaps, be a blatant call for more sophisticated models that take into account structure-dependent GB properties.

#### 4. Conclusions

In this work the origin of the transition in the dominant deformation mechanism from twinning to slip in pure Mg with grain refinement, with decreasing strain rate and with increasing temperature is investigated. With that aim, compression tests at a wide range of strain rates and temperatures were performed in two rolled and annealed polycrystals with grain sizes of 19 and 5 μm. The twin and slip activities were estimated by an exhaustive EBSD-assisted slip trace analysis study. The following conclusions can be drawn from the present study:

- (1) A transition from twinning to basal slip dominated flow takes place at 50 °C and  $10^{-3}$  s $^{-1}$  when the grain size is reduced from 19 to 5 μm. In the fine grained polycrystal strain is accommodated predominantly by basal slip taking place along well defined deformation bands. The origin of the transition lays on the differences in the GB networks of the two polycrystals emerging from the processing and, more precisely, in the higher connectivity between grains that are favorably oriented for basal slip present in the fine grained polycrystal.
- (2) A similar transition from twinning to basal slip dominated flow takes place at 50 °C when the strain rate is decreased from  $10^{-3}$  to  $10^{-5}$  s $^{-1}$  and at  $10^{-3}$  s $^{-1}$  when the temperature is increased from 50 to 150 °C. It is shown how this transition is due to the relaxation of constraints at GBs with decreasing strain rate and increasing temperature, leading to better connectivity between grains that are favorably oriented for basal slip.
- (3) At  $10^{-3}$  s $^{-1}$  and 250 °C basal slip is still the dominant deformation mechanism but the contribution to strain of non-basal slip increases noticeably due to the well-known decrease of the CRSS of prismatic and pyramidal systems with temperature as well as to enhanced cross-slip from basal to non-basal planes.
- (4) The current study suggests that the topology of the GB network, and the nature of individual GBs, together with the spatial distribution of orientations, play a decisive role in the selection of the dominant deformation mechanisms in pure Mg polycrystals, hinting that care must be taken when relating bulk mechanical properties with average grain size values.

#### Acknowledgements

The authors wish to acknowledge financial support from the European Commission (ExoMet Project, 7th Framework Programme, contract FP7-NMP3-LA-2012-280421). The research leading to these results has also received funding from Madrid region under programme S2013/MIT-2775, DIMMAT project. Prof. Oscar Ruano (CENIM-CSIC, Madrid) is sincerely thanked for allowing the use of the rolling equipment for this research work.

#### References

- [1] J.W. Christian, S. Mahajan, *Prog. Mater. Sci.* 39 (1995) 1.
- [2] G.I. Taylor, *J. Inst. Met.* 62 (1938) 307.
- [3] A. Chapuis, J.H. Driver, *Acta Mater.* 59 (2011) 1986.
- [4] J. Zhang, S.P. Joshi, *J. Mech. Phys. Solids* 60 (2012) 945.
- [5] C. Bettles, M. Barnett (Eds.), *Advances in Wrought Magnesium Alloys*, Woodhead publishing, Cambridge, 2012.
- [6] M.A. Meyers, O. Vohringer, V.A. Lubarda, *Acta Mater.* 49 (2001) 4025.
- [7] M.R. Barnett, Z. Keshavarz, A.G. Beer, D. Atwell, *Acta Mater.* 52 (2004) 5093.
- [8] M.R. Barnett, *Scr. Mater.* 59 (2008) 696.
- [9] B. Racisinia, S.R. Agnew, *Scr. Mater.* 63 (2010) 731.
- [10] H. Somekawa, T. Mukai, *Mater. Sci. Eng. A* 561 (2013) 378.
- [11] J. Bohlen, P. Dobroň, J. Swiostek, D. Letzig, F. Chmelik, P. Lukáč, K.U. Kainer, *Mater. Sci. Eng. A* 462 (2007) 302.
- [12] R.W. Armstrong, *Can. Metall. Q.* 13 (1974) 187.
- [13] N. Stanford, M.R. Barnett, *Int. J. Plast.* 47 (2013) 165.
- [14] C.H. Cáceres, G.E. Mann, J.R. Griffiths, *Metall. Mater. Trans. A* 42 (2011) 1950.
- [15] Y. Wang, H. Choo, *Acta Mater.* 81 (2014) 83.
- [16] I.J. Beyerlein, L. Capolungo, P.E. Marshall, R.J. McCabe, C.N. Tomé, *Philos. Mag.* 90 (2010) 2161.
- [17] P. Dobron, F. Chmelik, S. Yi, K. Parfenenko, D. Letzig, J. Bohlen, *Scr. Mater.* 65 (2011) 424.
- [18] A. Jain, O. Duygulu, D.W. Brown, C.N. Tomé, S.R. Agnew, *Mater. Sci. Eng. A* 486 (2008) 545.
- [19] J. Li, W. Xu, X. Wu, H. Ding, K. Xia, *Mater. Sci. Eng. A* 528 (2011) 5993.
- [20] H.J. Choi, Y. Kim, J.H. Shin, D.H. Bae, *Mater. Sci. Eng. A* 527 (2010) 1565.
- [21] Y. Chino, K. Kimura, M. Mabuchi, *Mater. Sci. Eng. A* 486 (2008) 481.
- [22] A. Ghaderi, M.R. Barnett, *Acta Mater.* 59 (2011) 7824.
- [23] O. Muránsky, M.R. Barnett, D.G. Carr, S.C. Vogel, E.C. Oliver, *Acta Mater.* 58 (2010) 1503.
- [24] X.L. Wu, K.M. Youssef, C.C. Kock, S.N. Mathaudu, L.J. Kekskés, Y.T. Zhu, *Scr. Mater.* 64 (2011) 213.
- [25] A.S. Khan, A. Pandey, T. Gnäupel-Herold, R.K. Mishra, *Int. J. Plast.* 27 (2011) 688.
- [26] N.V. Dudamell, I. Ulacia, F. Gálvez, S.B. Yi, J. Bohlen, D. Letzig, I. Hurtado, M.T. Pérez-Prado, *Acta Mater.* 59 (2011) 6949.
- [27] I. Ulacia, N.V. Dudamell, F. Gálvez, S. Yi, M.T. Pérez-Prado, I. Hurtado, *Acta Mater.* 58 (2010) 2988.
- [28] K. Ishikawa, H. Watanabe, T. Mukai, *Mater. Lett.* 59 (2005) 1511.
- [29] K. Ishikawa, H. Watanabe, T. Mukai, *J. Mater. Sci.* 40 (2005) 1577.
- [30] H. Watanabe, K. Ishikawa, T. Mukai, *Key Eng. Mater.* 340–341 (2007) 107.
- [31] H. Watanabe, K. Ishikawa, *Mater. Sci. Eng. A* 523 (2009) 304.
- [32] A. Jain, S.R. Agnew, *Mater. Sci. Eng. A* 462 (2007) 29.
- [33] F. Kabirian, A.S. Khan, T. Gnäupel-Herold, *Int. J. Plast.* 68 (2015) 1.

- [34] Q. Ma, B. Li, A.L. Oppedal, W.R. Whittington, S.J. Horstemeyer, E.B. Marin, P.T. Wang, M.F. Horstemeyer, Mater. Sci. Eng. A 559 (2013) 314.
- [35] T. Al-Sammam, X. Li, S. Ghosh Chowdhury, Mater. Sci. Eng. A 527 (2010) 3450.
- [36] M.R. Barnett, Metall. Mater. Trans. A 34 (2003) 1799.
- [37] D.B. Williams, C.B. Carter, Transmission Electron Microscopy, Plenum Press, 1996.
- [38] C.M. Cepeda-Jiménez, J.M. Molina-Aldareguia, M.T. Pérez-Prado, Acta Mater. 84 (2015) 443.
- [39] C.J. Boehlert, Z. Chen, I. Gutiérrez-Urrutia, J. Llorca, M.T. Pérez-Prado, Acta Mater. 60 (2012) 1889.
- [40] C.J. Boehlert, H. Li, L. Wang, B. Bartha, Adv. Mater. Processes 168 (2010) 41.
- [41] T.R. Bieler, P. Eisenlohr, F. Roters, D. Kumar, D.E. Mason, M.A. Crimp, D. Raabe, Int. J. Plast. 25 (2009) 1655.
- [42] M.R. Barnett, Mater. Sci. Eng. A 464 (2007) 1.
- [43] M.D. Nave, M.R. Barnett, Scr. Mater. 51 (2004) 881.
- [44] S.-G. Hong, S.H. Park, C.S. Lee, Acta Mater. 58 (2010) 5873.
- [45] M.R. Barnett, M.D. Nave, A. Ghaderi, Acta Mater. 60 (2012) 1433.
- [46] A. Fernández, M.T. Pérez-Prado, Y. Wei, A. Jérusalem, Int. J. Plast. 27 (2011) 1739.
- [47] A. Fernández, A. Jérusalem, I. Gutiérrez-Urrutia, M.T. Pérez-Prado, Acta Mater. 61 (2013) 7679.
- [48] C.A. Schuh, M. Kumar, W. King, Acta Mater. 51 (2003) 687.
- [49] B.W. Reed, C.A. Schuh, in: A.J. Schwartz, M. Kumar, B.L. Adams, D.P. Field (Eds.), Electron Backscatter Diffraction in Materials Science, Springer, 2009, p.205.
- [50] V.Y. Gertsman, M. Janecek, K. Tangri, Acta Mater. 44 (1996) 2869.
- [51] J.A. Del Valle, F. Carreño, O.A. Ruano, Acta Mater. 54 (2006) 4247.
- [52] D.L. Yin, J.T. Wang, J.Q. Liu, X. Zhao, J. Alloys Compd. 478 (2009) 789.
- [53] D.L. Atwell, M.R. Barnett, W.B. Hutchinson, Mater. Sci. Eng. A 549 (2012) 1.
- [54] M.R. Barnett, M.D. Nave, C.J. Bettles, Mater. Sci. Eng. A 386 (2004) 205.
- [55] F. Wang, S. Sandlöbes, M. Diehl, L. Sharma, F. Roters, D. Raabe, Acta Mater. 80 (2014) 77.
- [56] S.E. Ion, F.J. Humphreys, S.H. White, Acta Metall. 30 (1982) 1909.
- [57] J.A. Del Valle, M.T. Pérez-Prado, O.A. Ruano, Mater. Sci. Eng. A 355 (2003) 68.
- [58] J.A. Yasi, L.G. Hector, D.R. Trinkle, Acta Mater. 59 (2011) 5652.